PHYSOR 2014 - The Role of Reactor Physics toward a Sustainable Future
The Westin Miyako, Kyoto, Japan, September 28 - October 3, 2014, on CD-ROM (2014)

DEVELOPMENT OF A THREE-DIMENSIONAL KINETICS CODE FOR COMMERCIAL-SCALE FBR FULL CORE ANALYSIS.

Y. Shimazu, T. Takeda, W.F.G. van Rooijen*
Research Institute of Nuclear Engineering
University of Fukui, Tsuruga, Fukui, Japan
shimazu,t_takeda,rooijen@u-fukui.ac.jp

ABSTRACT

A transient analysis code has been developed for the analysis of future, commercial-size Fast Breeder Reactors. The code uses diffusion theory, a nodal expansion method for the spatial discretization, while the temporal discretization uses either a direct numerical solution, the Improved Quasi-Static method, or the adiabatic method. Numerical acceleration is used to obtain practical calculation times on large problems. Trial calculations have shown satisfactory code performance

Key Words: **Fast Breeder Reactor, Transient Analysis, Numerical Analysis, Monju, Improved Quasi-Static, Adiabatic**

1. INTRODUCTION

The core designs of advanced Fast Breeder Reactors (FBR) have features which cannot be modeled (accurately) with existing simulation tools. For this reason, a multi-year R&D project, with partners from academia and industry, to develop advanced methods in the areas of neutronics, materials science and thermal hydraulics was performed.

The present paper discusses development work in the area of three dimensional neutron kinetic analysis of FBRs. There exists a kinetic code for FBR applications, developed in Japan by one of the authors: KICOM [1]. In the current work, the theory and models of KICOM were used to develop an improved code. Since the new code does not yet have an official name, we will refer to it as "present code" in this work. The code uses diffusion theory. Spatial discretization uses a Nodal Expansion Method, while the temporal discretization uses either a direct numerical solution of the time-dependent diffusion equation, the Improved Quasi-Static method (IQS), or the adiabatic method. Numerical acceleration is used to obtain practical calculation times for large problems. The code has an option to adaptively select the solution method for transients (IQS when needed, otherwise adiabatic), as well as automatic control of timing of the recalculation of the shape function. Trial calculations have shown satisfactory performance.

*More information on our homepage at http://www.rine.u-fukui.ac.jp/

2. THEORY

In this section will be presented some of the theoretical details of the present work. The spatial discretization is based on the Nodal Expansion Method (NEM). Several approximations the kinetic calculation are available.

2.1. Hexagonal Nodal Expansion Method

For hexagonal geometries, the NEM is developed by defining four axes: 3 axes in the horizontal plane at 60° angles (x, u, and v), and one vertical axis (z). For each of these directions a one-dimensional diffusion equation is defined by integrating the three dimensional diffusion equation over the transverse directions. Subsequently, the resulting one-dimensional fluxes in node k and direction d are expanded:

$$\varphi_{gd}^{k}(d) \equiv \frac{V_k}{\Delta d_k}\left[\overline{\varphi}_{g}^{k} + \sum_{n=1}^{N} a_{gdn}^{k} f_{dn}(d)\right], \quad N = 4, \quad d = (x, u, v, z) \tag{1}$$

where k is the node index and g the energy group index. In the present work, we have used $N = 4$ in the horizontal and vertical directions. In Table I we give the expansion functions $f_{dn}(d)$. The solution is found by determining the the coefficients a_{gdn}^{k}. This is achieved with an iterative non-linear method, taking into account the continuity of the flux and the current at the node boundary, as well as the balance of the zero'th, first and second order flux moments in the node.

Table I. Expansion functions $f_{dn}(d)$ used as nodal expansion functions.

	Horizontal ($d = x, u, v$)	Vertical ($d = z$)
f_{d1}	$\frac{d}{h}$	$\frac{z}{h}$
f_{d2}	$\frac{36}{13}\left(\frac{d}{h}\right)^2 - \frac{5}{26}$	$3\left(\frac{z}{h}\right)^2 - \frac{1}{4}$
f_{d3}	$\frac{10}{13}\left(\frac{d}{h}\right)^2 - \frac{1}{2}\left\|\frac{d}{h}\right\| + \frac{3}{52}$	$\frac{z}{h}\left(\frac{z}{h} - \frac{1}{2}\right)\left(\frac{z}{h} + \frac{1}{2}\right)$
f_{d4}	$\frac{d}{h}\left(\left\|\frac{d}{h}\right\| - \frac{1}{2}\right)$	$\left(\frac{z}{h}\right)^4 - \frac{3}{10}\left(\frac{z}{h}\right)^2 + \frac{1}{80}$

2.2. Solution Methods for the Time-Dependent Diffusion Equation

There are several approximative methods to solve the time-dependent diffusion (or transport) equation. Since the present work uses several of these methods, a short introduction is given here. Details are readily available in textbooks, for instance [2]. First, the time-dependent neutron flux is factorized into the product of an amplitude and a shape funtion, i.e.

$$\varphi(\mathbf{r}, E, t) = p(t)\psi(\mathbf{r}, E, t)$$

Since one introduces an extra degree of freedom by this factorization, an extra normalization condition is needed. Upon substitution of the flux factorization into the diffusion equation, one obtains two coupled equations for the amplitude function $p(t)$:

$$\dot{p}(t) = \frac{\rho(t) - \beta(t)}{\Lambda(t)} p(t) + \frac{1}{\Lambda(t)} s_d(t) \tag{2}$$

and the shape function $\psi(\mathbf{r}, E, r)$:

$$\left[\mathbf{F}_p - \mathbf{M}\right] \psi(\mathbf{r}, E, t) + \frac{1}{p(t)} S_d(t; t') = \frac{1}{v}\frac{\dot{p}}{p}\psi(\mathbf{r}, E, t) + \frac{1}{v}\frac{\partial}{\partial t}\psi(\mathbf{r}, E, t) \tag{3}$$

Symbols: s_d is the reduced delayed neutron source; $\mathbf{F}_p$ is the prompt fission operator; $\mathbf{M}$ is the migration and loss operator; $S_d(t; t')$ is the source of delayed neutrons at time t due to the irradiation history t', and v is the velocity of the neutron. These coupled equations are solved simultaneously. In practice, the time step for the solution of the amplitude function $p(t)$, call it Δt_p, is chosen to be (much) smaller than the time step Δt_s for the solution of the shape function $\psi(\mathbf{r}, E, t)$. Subsequent approximations and simplifications can be made, resulting in several solution methods. In decreasing order of accuracy:

- Approximate the time derivative of the shape function at time t_k as:

$$\frac{\partial}{\partial t}\psi(\mathbf{r}, E, t) \approx \frac{1}{\Delta t_s}\left[\psi(\mathbf{r}, E, t_k) - \psi(\mathbf{r}, E, t_{k-1})\right]$$

  What results is the *Improved Quasi-Static Method* (IQS):

$$\left(\mathbf{F}_p - \mathbf{M} + \frac{1}{v\Delta t_s} - \frac{1}{v}\frac{\dot{p}}{p}\right)\psi(\mathbf{r}, E, t_k) = -\frac{1}{p} S_d(t_k; t') + \frac{1}{v\Delta t_s}\psi(\mathbf{r}, E, t_{k-1}) \tag{4}$$

- If one uses $\partial\psi/\partial t = 0$, one finds the *Quasi-Static Method*:

$$\left(\mathbf{F}_p - \mathbf{M} - \frac{1}{v}\frac{\dot{p}}{p}\right)\psi(\mathbf{r}, E, t_k) = -\frac{1}{p} S_d(t_k; t') \tag{5}$$

- If we go one step further, and assume that the delayed neutron source at time t_k is simply a fraction of the total fission source, and neglect the $(1/v)\cdot(\dot{p}/p)$-term, one finds the so-called *Adiabatic Method*. In this case, the equation of the shape function reduces to a static form, and an eigenvalue must be introduced to find a non-trivial solution:

$$(\mathbf{M}-\lambda\mathbf{F})\,\psi(\mathbf{r},E,t_k)=0 \tag{6}$$

- If we also neglect the fact that the operators $\mathbf{M}$ and $\mathbf{F}$ are time-dependent, we find the *Point Kinetics Equation*, i.e. the shape function is found from:

$$(\mathbf{M}_0-\lambda_0\mathbf{F}_0)\,\psi_0(\mathbf{r},E)=0 \tag{7}$$

  and is not updated.

These approximations are commonly used in kinetics codes. However, in certain cases it is important to have the possibility to perform reference calculations. For this, a direct numerical solution of the diffusion equation has been implemented in our new code. For the direct solution, consider the time dependent neutron diffusion equation and the equations for the concentration of delayed neutrons:

$$\frac{1}{v_g}\frac{\partial\varphi^g}{\partial t}-\nabla\cdot D^g\nabla\varphi^g+\Sigma_t^g\varphi^g=\sum_{g'=1}^{G}\Sigma_s^{g\leftarrow g'}\varphi^{g'}+\chi_p^g(1-\beta)\sum_{g'=1}^{G}\nu\Sigma_f^{g'}\varphi^{g'}+\sum_{k=1}^{K}\chi_{d,k}^g\lambda_k C_k \tag{8}$$

$$\frac{\partial C_k}{\partial t}=\beta_k\sum_{g=1}^{G}\nu\Sigma_f^g\varphi^g-\lambda_k C_k \tag{9}$$

and appropriate boundary conditions in space and time are implicitly assumed. Use a fully implicit discretization for the time derivative:

$$\frac{1}{v_g}\frac{\partial\varphi^g}{\partial t}\Big|_{t_n}=\frac{\varphi(t_{n+1})-\varphi(t_n)}{v_g\Delta t_n},\qquad\text{with}\quad\Delta t_n=t_{n+1}-t_n \tag{10}$$

then the discretized version of the time-dependent diffusion equation is found as:

$$\begin{aligned}&-\nabla\cdot D^g\nabla\varphi^g(t_{n+1})+\left(\Sigma_t^g+\frac{1}{v_g\Delta t_n}\right)\varphi^g(t_{n+1})=\\&\sum_{g'=1}^{G}\Sigma_s^{g\leftarrow g'}\varphi^{g'}(t_{n+1})+\frac{\chi_p^g(1-\beta)}{k_0}\sum_{g'=1}^{G}\nu\Sigma_f^{g'}\varphi^{g'}(t_{n+1})+\sum_{k=1}^{K}\chi_{d,k}^g\lambda_k C_k(t_{n+1})+\frac{\varphi^g(t_n)}{v_g\Delta t_n}\end{aligned} \tag{11}$$

For the precursor concentrations, one obtains:

$$C_k(t_{n+1}) = C_k(t_n)e^{-\lambda_k \Delta t_n} + \frac{\beta_k}{k_0} \int_{t_n}^{t_{n+1}} \sum_{g=1}^{G} \nu\Sigma_f^g \varphi^g(t') e^{-\lambda_k (t_{n+1}-t')} \, \mathrm{d}t' \tag{12}$$

In these equations, a multiplication factor k_0 is introduced to enforce an initial steady state. If the time step Δt_n is small enough, we can assume a linear variation of the flux between t_n and t_{n+1}:

$$\nu\Sigma_f^g \varphi^g(t') \equiv F(t') = F(t_n) + \frac{F(t_{n+1}) - F(t_n)}{\Delta t_n}(t' - t_n) \tag{13}$$

From which we find:

$$C_k(t_{n+1}) = C_k(t_n)e^{-\lambda_k \Delta t_n} + a_1 \frac{\beta_k}{k_0} \sum_{g=1}^{G} \nu\Sigma_f^g \varphi^g(t_{n+1}) + a_0 \frac{\beta_k}{k_0} \sum_{g=1}^{G} \nu\Sigma_f^g \varphi^g(t_n) \tag{14}$$

$$a_1 = \frac{1}{\lambda_k \Delta t_n} \left(\Delta t_n - \frac{1 - e^{-\lambda_k \Delta t_n}}{\lambda_k} \right) \tag{15}$$

$$a_0 = -a_1 + \frac{1 - e^{-\lambda_k \Delta t_n}}{\lambda_k} \tag{16}$$

One can now combine Equations (11) and (14). The resulting equation contains $\varphi^g(t_{n+1})$, $\varphi^g(t_n)$ and $C_k(t_n)$, and can thus be interpreted as a source-driven diffusion equation with modified cross sections, where $\varphi^g(t_n)$ and $C_k(t_n)$ appear as source terms. Once the new flux $\varphi^g(t_{n+1})$ is calculated, the new precursor densities $C_k(t_{n+1})$follow from Eq. (14). This method is similar to the work presented in Ref. [3].

2.3. Acceleration and Temperature Model

Initial calculations showed that the calculation time was too long for practical applications. It was chosen to implement several acceleration methods:

- For the forward and adjoint eigenvalue calculations (needed to derive various parameters for the kinetic approximations): Wielandt eigenvalue shift method, Chebychev-acceleration and flux extrapolation.
- For the transient (i.e. not eigenvalue) calculations: Chebychev-acceleration and flux extrapolation.

Using the Wielandt, Chebychev and flux-extrapolation accelerations, an overall acceleration factor of about 4 to 5 was achieved for the eigenvalue calculations in forward and adjoint mode. For transient cases the Wielandt-method is not available, but application of the Chebychev acceleration and flux extrapolation resulted in an acceleration factor of about 4. These results are satisfactory.

For both eigenvalue and transient calculations, one needs to perform many fixed-source calculations. We have implemented the LIS [4] solvers focusing on implementation on parallel computers. LIS solvers were applied either at the within-group level (i.e. spatial flux solution for one energy group), or at the multi-group level (i.e. the sweep over the energy groups). For the eigenvalue calculation, which is based on the clasic "inner-outer" scheme, very good performance was found for the BiCGSTAB-solver. For the transient case, the same solver was applied to solve the flux, treating all energy groups simultaneously. This calculation, which can be unstable in the conventional implementation, was shown to be stable and efficient with BiCGSTAB.

Feedback effects due to temperature require a thermohydraulic model. A thermal model based on a single pin and its associated coolant channel has been implemented and the performance compared to the COBRA-IV code [5]. In general, accuracy is satisfactory.

2.4. Timing of the Shape Function Calculation

In both the IQS method and the adiabatic method the shape function $\psi(\mathbf{r}, E, t)$ needs to be recalculated from time to time. For optimal performance, the timing of the recalculation has been automated in our code. The shape function is recalculated if any of the following conditions are met:

- If one assumes an exponential increase of the power, i.e. $p(t) = p_0 \exp(t/T)$, then one can define the *period* T_n of time step n from:

$$\frac{n_n}{n_{n-1}} = e^{\frac{\Delta t_n}{T_n}} \Rightarrow \ln\left(\frac{n_n}{n_{n-1}}\right) = \frac{\Delta t_n}{T_n}$$

  If $T_n - T_{n-1} > 1.0 \times 10^6$, the shape function is recalculated.

- Recalculation if $-C \leq \log(\Delta t_n / \Delta t_{n-1}) \leq C$ is not fulfilled, where C a user-defined constant (default 0.2).

- Define the assembly integrated power error of assembly i at time step n as:

$$E_{i,n} = 1 - \frac{\int P_{i,n}(z)dz}{\int P_{i,n-1}(z)dz}$$

  and let E_{max} be the largest error over all assemblies, and E_{min} the minimum error. Recalculate if $E_{\text{max}} - E_{\text{min}} > K$, where K is a user-defined constant.

- Recalculate if the time step Δt_n is larger than a user-defined value.
- Finally, a recalculation is always done in the following cases: (1) at the end of control rod movement; (2) the first two steps of the calculation; (3) at the end of the transient.

2.5. Solution Method Selection

The IQS method is more accurate than the adiabatic method, but requires a longer calculation time. Therefore, it is beneficial to use the adiabatic method whenever possible. In our code, the solution method is selected as follows:

- During control rod movement: IQS method
- Otherwise: select method based on reactivity; choose IQS if reactivity is larger than a user-defined value, use adiabatic method otherwise

3. RESULTS

In this section the results of several trial calculations are illustrated. First, the results of static problems are given; following are the results for the direct numerical kinetic solutions (kinetic problems). Finally, we give the results for calculations with feedback (dynamic problems), with automatic selection of solution method and timing.

3.1. Results for Static Problems

In Table II we give an overview of the results for eigenvalue problems, comparing the code developed in the present work and DIF3D. Calculations are done for a 2D hexagonal geometry and a 3D Hex-Z geometry. As can be seen, in general an excellent agreement is found between the newly developed code and the reference codes. For the 3D case, the result from the new code with four expansion terms along the z-direction ($N_z = 4$) is more precise than the DIF3D result, which uses only 3 expansion terms ($N_z = 3$).

3.2. Results for Kinetic Problems

3.2.1. Thermal reactor, 2D calculation

The test cases are the same as those used in the verification of DIF3D [6]. These calculations are in turn based on work published earlier [7]. In Ref. [6] the required data for these calculations is given,

Table II. Comparison between our code and DIF3D for eigenvalue calculations. 2D and 3D hexagonal calculations. The DIF3D reference case uses a triangular mesh with extrapolation to zero mesh size. Nodal calculations performed with one node per hexagon.

2D Hexagonal		3D Hexagonal-Z	
Code	k_{eff}	Code	k_{eff}
DIF3D reference	1.0718	DIF3D reference	0.99459
DIF3D nodal	1.0731	DIF3D nodal	0.99538
New code, nodal	1.0731	New code, nodal, $N_z = 3$	0.99538
		New code, nodal, $N_z = 4$	0.99491

i.e. homogenized cross sections, delayed neutron data, etc. Two cases are reported, named *PDP-Case-1* and *PDP-Case-2*. Both test cases use a core made of hexagonal assemblies with various compositions. The core has a 60° symmetry. In Case-1, a total of 12 assemblies are perturbed, two per 60°-sector. These assemblies are located in a high flux position away from the core center. This perturbation has a high locality. Case-2 uses the same core, but a larger perturbation of 133 assemblies in the core center. At the onset of the transient, the thermal absorption cross section in the core center is reduced by 4.5% in 0.2 s. This perturbation has a low locality. The details of these transients are given in Table III.

In Figs. 1 and 2 are shown the results for the reactor power for PDP-Case-1 and PDP-Case-2, respectively. For the new code, results of IQS calculations as well as the direct numerical solution are given. It is seen that in this case there is not much difference. Results for DIF3D and FX2-TH[1] are given only at the end of the transient ($t = 5$ s). Our new code and DIF3D agree quite well, but the result from FX2-TH is rather different. This is attributed to a too large mesh size in the FX2-TH calculation [6].

Table III. Main parameters of the 2D thermal reactor test cases.

Items	PDP-Case-1	PDP-Case-2
Perturbation	12 SAs, high flux position	133 SAs in the core center
Input	Fuel bearing rods introduced	4.5% reduction of thermal absorption cross section
# Energy groups	2	2
# Delay groups	6	6
Perturbation locality	High	Low

[1] FX2-TH: a code to solve the steady-state and time-dependent two-dimensional multigroup neutron diffusion equations with thermal and hydraulic feedback. Published 1978, Argonne National Laboratory, and available through RSICC.

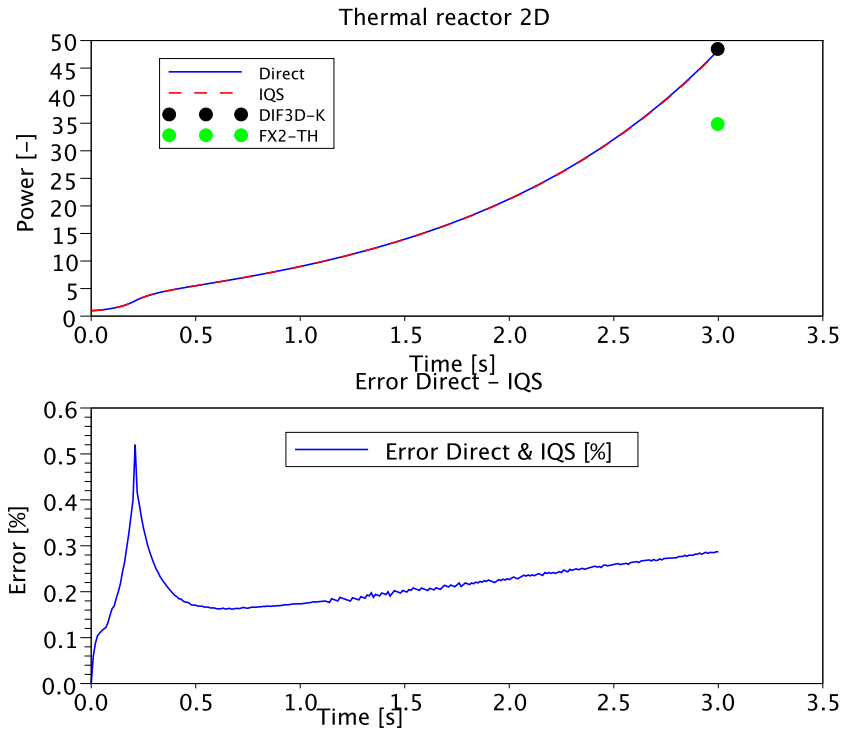

Figure 1. PDP-Case-1: power and associated error (left).

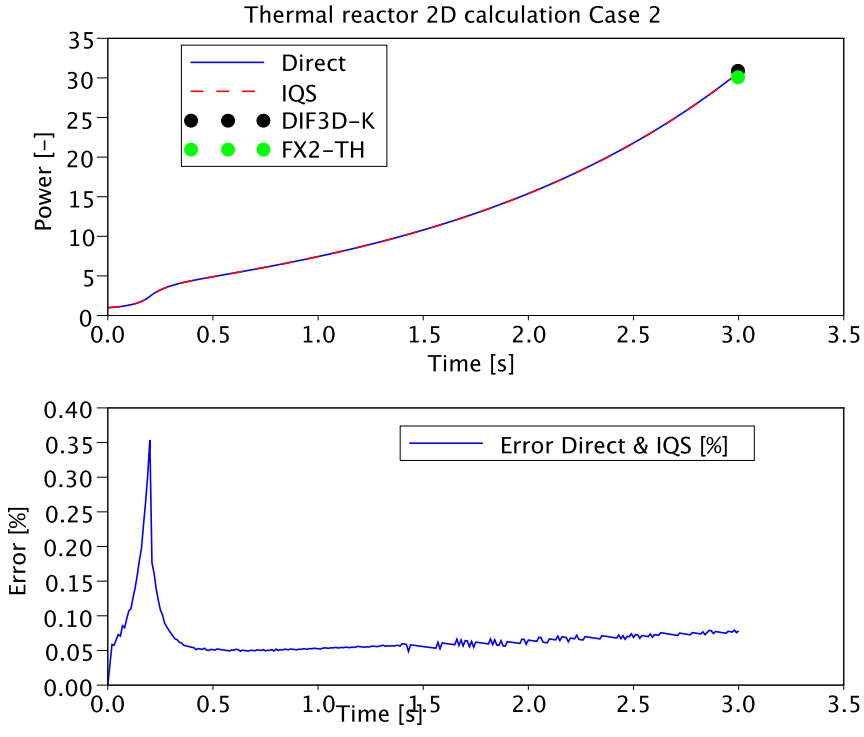

Figure 2. PDP-Case-2: power and associated error.

Table IV. Main parameters of the thermal reactor 3D test case.

Items	
Perturbation	7 assemblies in the core center
Input	Step reduction of thermal absorption cross section by 15.37%
Energy groups	2
Delay groups	6
Perturbation locality	Low

3.2.2. Thermal reactor, 3D calculation

This test case is also taken from Ref. [6], which in turn is based on Ref. [7]. In this calculation, a rather substanstial perturbation is applied to the center of the core, namely a reduction of the thermal absorption cross section by 15%, resulting in a rapid increase of the power (factor of 135 in 5 s). The details of the thermal reactor 3D benchmark are given in Table IV.

In Figs. 3 and 4 are given the result for the reactor power and the flux distribution, respectively. Compared to DIF3D, the new code performs well in this case also. The error in the flux distribution becomes rather large at the outer boundary of the calculational domain (radial position 14 and 15). Since the outer regions of the reactor represent a region of low interest, and the flux is very low in this position, the error is deemed to be acceptable.

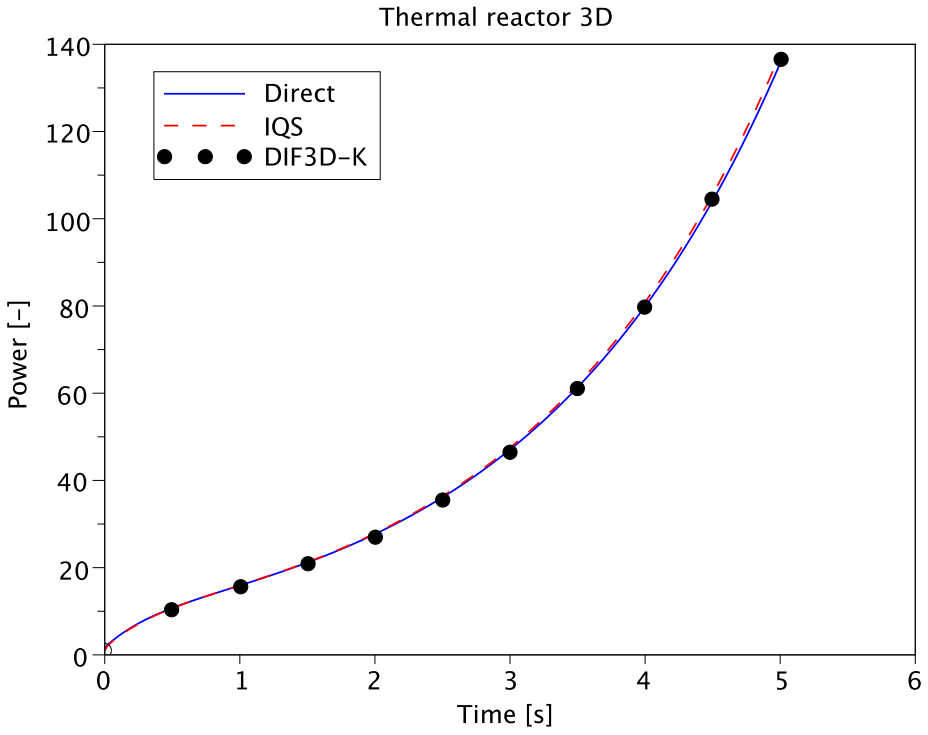

Figure 3. Thermal reactor 3D test case: power.

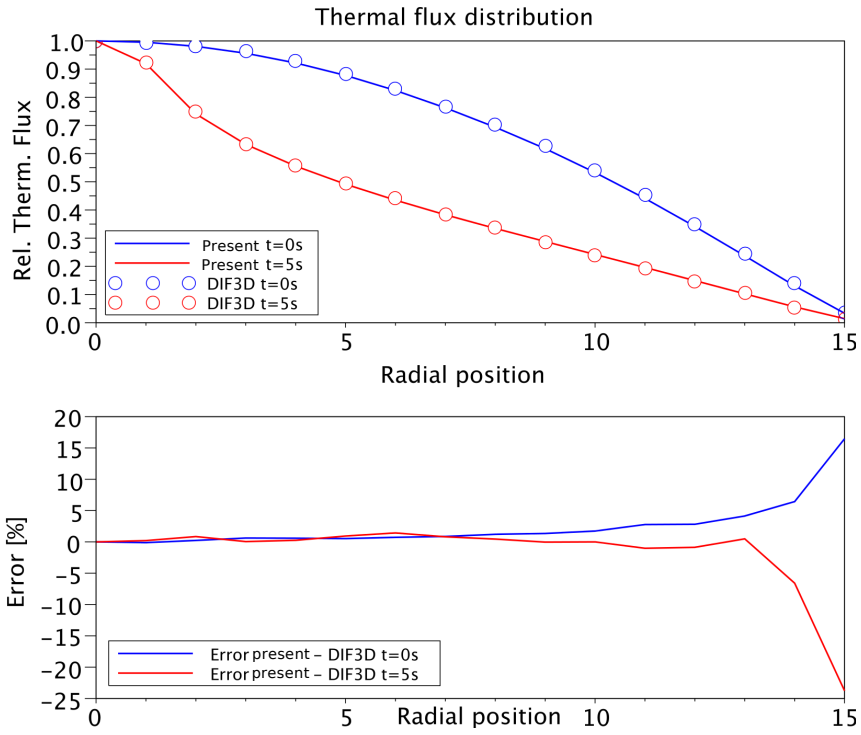

Figure 4. Thermal reactor 3D test case: thermal flux distribution at the start and end of the transient, and the associated error. The flux error becomes somewhat large in the near the outer boundary of the model, but here the fluxes are generally low, so the accuracy is deemed to be acceptable.

3.3. Results for Dynamic Problems

We present the results of two trial calculations. The first calculation is based on a reactor model similar to the prototype FBR Monju. The model used for the feedback calculation is based on one, "average" fuel pin, and its associated coolant channel. The fuel is a MOX fuel, with a cylindrical pellet, clad with stainless steel. The coolant is liquid sodium. In this calculation, the reactor is assumed to be critical at very low power. A rather large reactivity is introduced by removing the central control rod by 10 cm in 1 second, giving a reactivity of about 0.5$. This transient was calculated over a period of 50 minutes, but in the graphs only the first 6 minutes are shown. In Figure 5 is given the result of the calculation. The transient is calculated two times: one time with IQS only, and one time with the adaptive method, which switches between IQS and adiabatic. In both cases, the maximum time between shape function calculations was set to 20 seconds. The calculation with the IQS method requires 73 minutes; if the adiabatic option is used, the calculation requires 22 minutes.

In Figure 6 is given the result of the same calculation, where the timing of the shape function calculation is selected without user intervention. The IQS method is used.

The second result concerns the measurement of the Isothermal Temperature Coefficient of Monju. This measurement was performed in 2010, and is described in a JAEA report [8]. In this measurement, a small reactivity (approx. 6 cent) is introduced by moving the central control rod. The

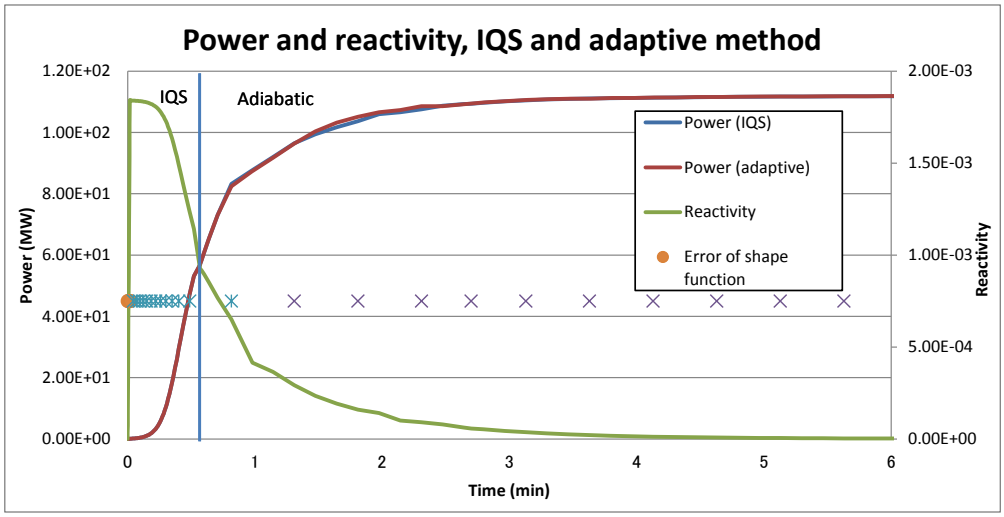

Figure 5. Transient in a typical FBR. The IQS method and the IQS/adiabatic methods are used. Symbols indicate the timing of the shape function calculations and the condition which caused the recalculation (see section 2.4.

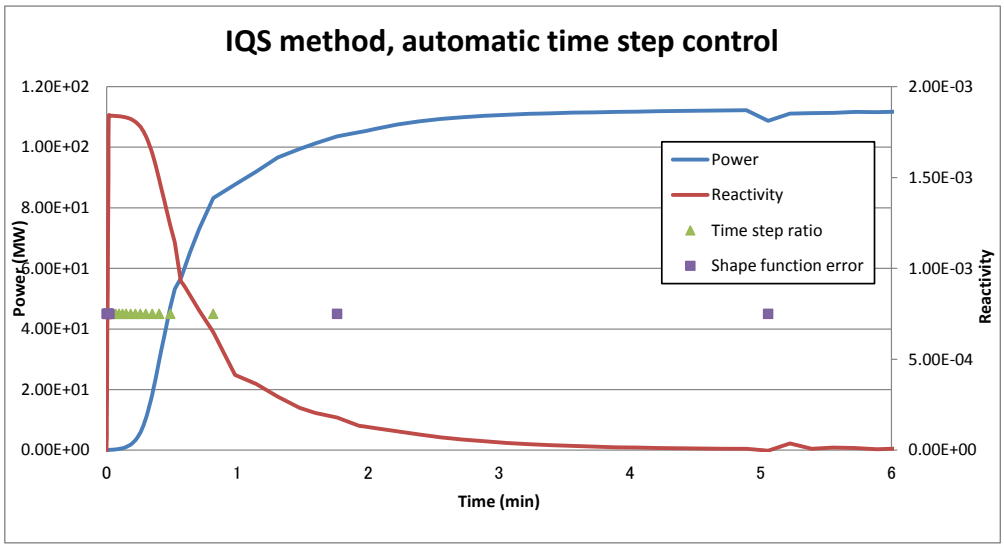

Figure 6. Transient in a typical FBR. The IQS method is used. Symbols indicate the timing of the shape function calculations and the condition which caused the recalculation (see section 2.4.

following transient is allowed to develop without further intervention for a period of several hours. Because of the very slow nature of this transient, the entire system remains in an isothermal condition. In Figure 7 is given the result of our calculation of the reactor power as well as the measured reactor power. During the first 20 seconds the IQS method is selected; from 20 seconds onwards, the adiabatic method is selected. In Figure 8 is given the reactivity: the inserted reactivity due to control rod movement (20 pcm (= 20.0×10^{-5}) corresponds to roughly 6 cents, $1\$ \approx 300$ pcm), the total reactivity, and the "external reactivity".

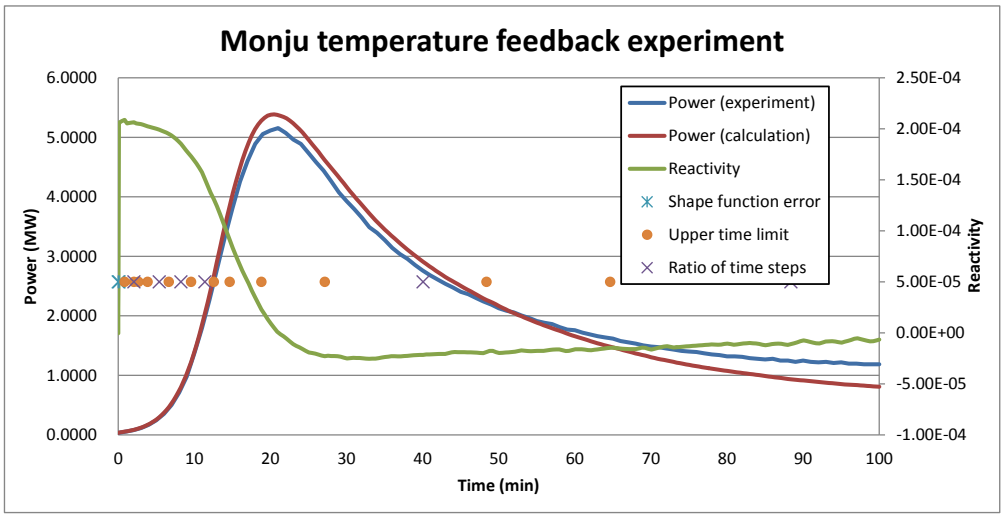

Figure 7. Measurement of the Isothermal Temperature coefficient in Monju. Given are the reactor power (experimental value and calculation), as well as the total reactivity. Symbols indicate the timing of the shape function calculations and the condition which caused the recalculation (see section 2.4.

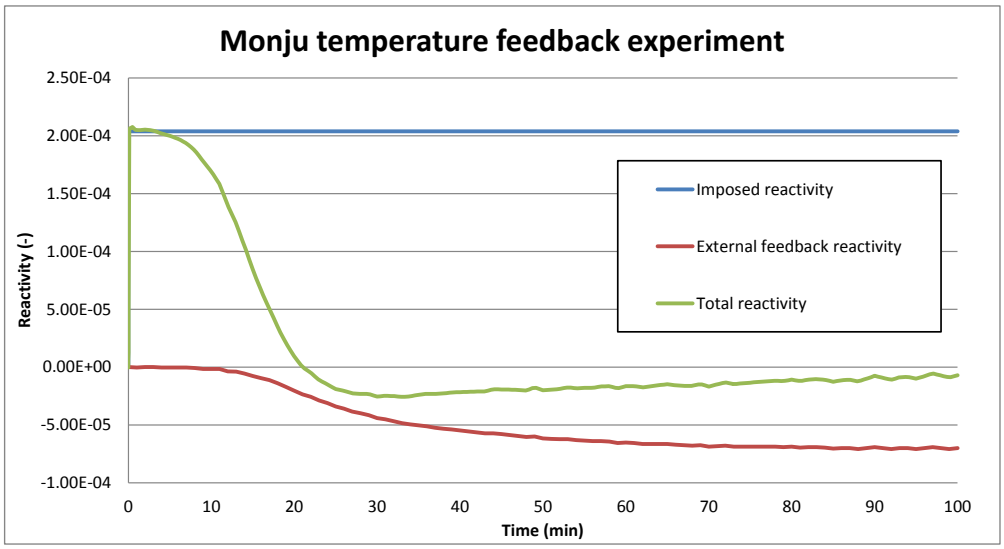

Figure 8. Measurement of the Isothermal Temperature coefficient in Monju. Given are the imposed reactivity due to control rod movement, the "external" reactivity as well as the total reactivity, which includes all feedback components.

The "external" feedback in Figure 8 is the reactivity feedback which is due to quantities which are not calculated in the thermal model. In the case of Monju, the thermal expansion of the grid plate is a source of feedback. Our code does not have a capability to take into account such a source of feedback. Therefore, a simplistic model was used, assuming that the reactivity feedback due to grid plate expansion is linear with the inlet temperature of the coolant. As can be seen in Figure 7 the C/E value becomes large towards the end of the calculation. There are two causes: one is the overly simplistic model of the grid plate expansion; in reality, the grid plate is a massive piece of stainless

steel, and the temperature of this component as well as it expansion state is a complex function of the mechanical and thermal coupling between the grid plate, the coolant, and the surrouding reactor components. The other source of deviation is the gap conductance between the pellet and the cladding. This is in important factor in the thermohydraulic analysis. Data in [8] is insufficient, so the magnitude of the gap conductance was adjusted to give an acceptable result.

4. CONCLUSION

For the accurate analysis of kinetic transients (without feedback) and limited dynamic transients (with feedback), a new analysis code was developed focusing on the analysis of future commercial-size FBRs. The code uses diffusion theory, with a nodal expansion method to treat the spatial discretization, while the temporal discretization is handled by either a direct numerical solution of the diffusion equation, the Improved Quasi-Static method, or the adiabatic method. A simple thermal model based on one fuel pin and its associated coolant channel is available to take into account feedback effects. Several numerical acceleration methods are implemented to make the calculation time short enough for practical applications. For transients, the code has the option to adaptively choose the solution method (IQS when needed, adiabatic when sufficient), as well as adaptive timing of the recalculation of the shape function.

Trial calculations were performed with static problems, kinetic, and dynamic problems. Code performance on these (synthetic cases) is satisfactory: for static problems, the multiplication factor and flux distribution is satisfactorily calculated. For the dynamic problems, the measured transient in Monju could be calculated with sufficient accuracy. A precise comparison with other thermal-hydraulic codes for the heat transfer model (heat exchange coefficient, pressure drop, dimensionless quantities) has not yet been done, but will be part of the further verification and validation of the newly developed code.

ACKNOWLEDGMENTS

The work presented in this publication contains is the result of a part of the research project “Fundamental R&D program for the commercialization of Fast Breeder Reactor technology using Monju”, entrusted to the University of Fukui by the Ministry of Education, Culture, Sports, Science and Technology of Japan (MEXT) and executed from FY2009 to FY2012.

REFERENCES

[1] Toshikazu Takeda, Toshio Endo, and Hiroki Takaya. “Three-dimensional transient analysis of fast reactors with improved coarse mesh method.” *Journal of Nuclear Science and Technology*, **31(1)**: pp. 12 - 23 (1994).

[2] Karl O. Ott and Robert J. Neuhold. *Introductory Nuclear Reactor Dynamics*. ANS (1985).

[3] A. Pautz and A. Birkhofer. "DORT-TD: A transient neutron transport code with fully implicit time integration." *Nuclear Science and Engineering*, **145**: pp. 299 – 319 (2003).

[4] The Scalable Software Infrastructure Project. *LIS, a Libary of Iterative Solvers, v1.2.57, Users Manual*. URL http://www.ssisc.org (2011).

[5] C.W. Stewart *et al. COBRA-IV: The Model and the Method*, bnwl-2214 edition (1977).

[6] T.A. Taiwo and H.S. Khalil. "The DIF3D nodal kinetics capability in Hex-Z geometry - Formulation and preliminary tests." In: *Proc. Int. Conf. Advances in Mathematics, Computation and Reactor Physics, International topical meeting*. Greentree Marriott, Pittsburgh PA, USA (1991).

[7] M.R. Buckner and J.W. Stewart. "Multidimensional Space-Time Nuclear-Reactor Kinetics Studies." *Nuclear Science and Engineering*, **59**: p. 289 (1976).

[8] The technical committee on Monju research utilization. *External evaluation on Monju core confirmation test in FY2010. Technical Report JAEA-Evaluation 2011-002*, Japan Atomic Energy Agency. URL http://jolissrch-inter.tokai-sc.jaea.go.jp/pdfdata/JAEA-Evaluation-2011-002.pdf/ (2011).